19 Numerical Simulation Methods in Friction Physics

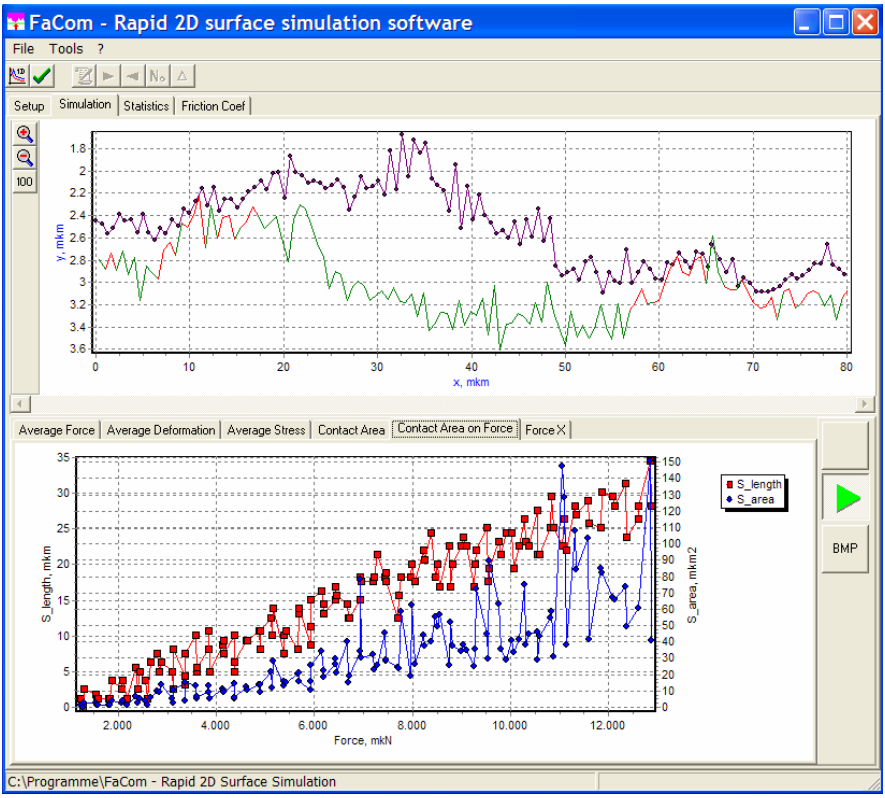

The contact and friction problems investigated in the previous chapters are based on simple model systems. Even when these models provide a general overview of complex tribological systems, a multitude of tribological problems, especially when they deal with the fine optimization of tribological systems, are not able to be calculated in analytical form. In these cases, researchers and engineers must fall back on numerical methods. At the same time, one must remember that the efficiency of numerical methods is dependent largely on the quality of the preceding analytical preparations.

In this chapter, we first present a short overview of the most important methods used in contact mechanics, describing them not in detail, but rather referring to existing literature. Only the fundamentals of one simulation method, the so-called "dimension reduction method," will be described in detail. This method can be used to simulate macroscopic tribological systems and, above all, the frictional forces in such systems, taking into account their "multi-scale character."

V.L. Popov, *Contact Mechanics and Friction,* DOI 10.1007/978-3-642-10803-7_19,

19.1 Simulation Methods for Contact and Frictional Problems: An Overview

19.1.1 Many-Body Systems

Computer simulations of many-body systems are indispensable for today's industrial development processes. With increasing demand on accuracy, the interest in reproducing contact and frictional phenomena as precise as possible is also increasing. A considerable part of research in this field is concentrated on finding methods for the implementation of simple contact conditions and Coulomb's law of friction. At the forefront, is the search for the most efficient algorithms possible (in terms of calculation time and implementation costs). Contact is typically seen as one-sided rigid constraint. For the laws of friction, there is assumed that there exists a maximum force of static friction and that the force of kinetic friction depend on sliding velocity. Frequently, the force of kinetic friction is assumed to be constant and equal to the maximum force of static friction.

The simplest method for integrating friction into many-body system programs is to approximate the law of friction using a continuous function of frictional force. The frictional force in treated as a given force for which the dependence on sliding velocity is known. Typically, a force in the following form is used (Fig. 19.1):

$$F_R = \frac{2}{\pi}\mu F_N \arctan\left(v/\hat{v}\right). \tag{19.1}$$

By using this form, one does not need to differentiate between static friction and kinetic friction. The characteristic velocity $\hat{v}$ must be chosen so that it is significantly smaller than the characteristic sliding velocity of the system to be simulated. In this case, the relation (19.1) expresses the behavior of the forces in both the stick and sliding domains[1].

[1] In this case, "sticking" is simply sliding at a very low velocity; the frictional force sets itself "automatically" equal to the correct force of static friction between $-\mu F_N$ and $+\mu F_N$. For many tribological applications, this "trick" corresponds even to the actual properties of the frictional force.

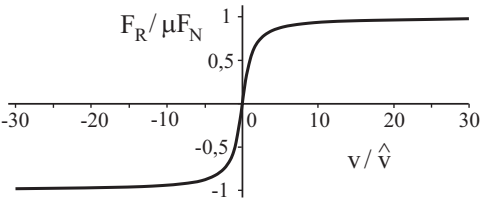

Fig. 19.1 Approximation of the law of friction by a continuous function of velocity.

19.1.2 Finite Element Methods

For many applications, the pressure distribution and the deformation of the contact interface are important. There are various simulation methods available for calculating elastic and plastic deformations, which give a principal possibility, to investigate adhesive contacts and frictional phenomena. Procedures based on discretizing the continuum equations are widely known, especially finite element methods (FEM) and boundary element methods.

Contact formulations in the framework of FEM were developed in the 1970's. Today, commercial FE-programs use the so-called *node-to-surface formulation*, which considers the nodes of the surface in relation to the elements of the other surface.

In many practical applications (seals, metal-forming processes, penetration tests), large deformations, non-linear behavior of materials, and large relative motion between the participating contact partners occur. In these cases, contact problems can be considerably more robustly and accurately simulated with *surface-to-surface formulation* (Mortar method)[2].

Rolling contact problems (wheel-rail, tire-street) are, likewise, investigated with the FE method. The *Arbitrary Lagrangian Eulerian* (ALE) method[3] is an effective method for calculating such contact problems. The spatially stationary discretization allows the resolution of the mesh for the contact areas to be refined. This is especially elegant in solving problems of steady state rolling, because the solution is time-independent in this case. However, taking inelastic material behaviors into account is difficult, because the mesh is not bound to the points of the material.

Advantages of a 3D-FE model are (1) the utilization of correct geometry (dimensions, surface topography, degrees of freedom) and (2) the ability to calculate

[2] M.A: Puso und T. A. Laursen, A mortar segment-to-segment contact method for large deformation solid mechanics. Computer Methods in Applied Mechanics and Engineering, 193:601-629, 2004.

[3] U. Nackenhorst, The ALE-formulation of bodies in rolling contact: theoretical foundations and finite element approach. Computer Methods in Applied Mechanics and Engineering, 193:4299-4322, 2004.

stresses and deformations in the entire body. Due to the very fine mesh, however, 3D-FE models require high processing times for rough surfaces. This is an especially clear disadvantage when regarding extensive parameter studies and optimizations. Thus, finite element methods are not practical for calculating frictional forces between rough surfaces.

19.1.3 Boundary Element Method

Boundary element method is especially suited for calculating contacts, because only the discretization of the surface is necessary. Because of the importance of this method in contact problems, we will discuss it in more detail. Here, we limit ourselves to normal contact problems between an elastic body and a rigid plane.

The vertical displacement of a point on the surface of an elastic body being acted upon by a continuous pressure distribution is given by (5.7). We divide the parts of the domain to be investigated into $N \times N$ elements and assume the pressure is constant in every individual element. The relation between pressure p_{ij} in a quadratic surface element and a vertical surface displacement u_{ij} can be analytically calculated:[4]

$$u_{ij} = \sum_{\tilde{i}=1}^{N} \sum_{\tilde{j}=1}^{N} K_{ij\tilde{i}\tilde{j}} p_{\tilde{i}\tilde{j}} \,, \tag{19.2}$$

with

$$\begin{aligned} K_{ij\tilde{i}\tilde{j}} = \frac{\Delta}{\pi E^*} \Bigg[& a \ln\left(\frac{c+\sqrt{a^2+c^2}}{d+\sqrt{a^2+b^2}} \right) + b \ln\left(\frac{d+\sqrt{b^2+d^2}}{c+\sqrt{b^2+c^2}} \right) \Bigg] + \\ & c \ln\left(\frac{a+\sqrt{a^2+c^2}}{b+\sqrt{c^2+b^2}} \right) + d \ln\left(\frac{b+\sqrt{b^2+d^2}}{a+\sqrt{a^2+d^2}} \right) \end{aligned} \tag{19.3}$$

and

$$\begin{aligned} a &= i - \hat{i} + \frac{1}{2} \quad , \quad b = i - \hat{i} - \frac{1}{2} \quad , \\ c &= j - \hat{j} + \frac{1}{2} \quad , \quad d = j - \hat{j} - \frac{1}{2} \quad . \end{aligned} \tag{19.4}$$

---

[4] A.E.H. Love, A Treatise on the Mathematical Theory of Elasticity. 4th edition., Cambridge, University Press. See also: K. L. Johnson, Contact mechanics. Cambridge University Press, 6th printing of the 1st edition, 2001, p. 54.

Δ is the mesh spacing. Equation (19.2) can be written in matrix form as

$$\mathbf{u} = \mathbf{A}\mathbf{p}\,, \tag{19.5}$$

with a matrix $\mathbf{A}$ with dimensions $N^2 \times N^2$. In contact problems, the size and location of the contact area is initially unknown. Therefore, contact problems must be solved iteratively. In the contact area, the separation between the surfaces is zero (i.e. in this area, the displacement of the elastic surface is known). Outside of the contact area, the pressure is zero; the displacement, on the other hand, is generally not zero. To begin, a contact area is assumed. The variables are now partitioned into the variables p_i and u_i inside of the contact area and p_a and u_a outside of the contact area. u_i and $p_a = 0$ are known. After rearranging according to (19.5), we obtain

$$\begin{bmatrix} \mathbf{A}_1 & \mathbf{A}_2 \\ \mathbf{A}_3 & \mathbf{A}_4 \end{bmatrix} \begin{Bmatrix} \mathbf{p}_\mathbf{i} \\ \mathbf{0} \end{Bmatrix} = \begin{Bmatrix} \mathbf{u}_\mathbf{i} \\ \mathbf{u}_\mathbf{a} \end{Bmatrix} \tag{19.6}$$

and finally,

$$\mathbf{A}_1\mathbf{p}_\mathbf{i} = \mathbf{u}_\mathbf{i}\,, \tag{19.7}$$

$$\mathbf{A}_3\mathbf{p}_\mathbf{i} = \mathbf{u}_\mathbf{a}\,. \tag{19.8}$$

The solution to the system of equations in (19.7) yields a pressure in the contact area of $\mathbf{p}_\mathbf{i}$. With these results, using (19.8), the displacement $\mathbf{u}_\mathbf{a}$ in the domain outside of the contact can be calculated. The first iteration step generally yields a negative pressure (tensile stress) in the contact area and a negative separation distance outside of the contact area. The new contact area is now chosen so that all of the points in tensile stress are removed from the contact area and all of the points with a negative separation difference are brought into it. With this new approximation of the contact area, the previously described calculation is repeated. The iteration continues until no more tensile stresses or negative separation distances exist (to a reasonable approximation).

19.1.4 Particle Methods

Another approach to the simulation of contact and frictional problems is provided by particle methods, for which discrete particles are the focus of the calculations. These particles are not real (physical) objects, rather purely "units for calculation." The interactions between the particles must be chosen so that the elastic and plastic behavior of the material is correctly described. Thus, neither the macroscopic continuum equations nor the microscopic equations of molecular dynamics are

solved, rather the microscopic equations of a suitable substitution system. The size of the particles can be adjusted to fit the problem. For example, for the investigation of earthquakes, the particle size can be on the order of meters.

The frictional force is determined by processes such as elastic and plastic deformation, fracture, and the dislodgement and reintegration of particles. These processes take place in micro-contacts. The *movable cellular automata* (MCA) method is a particle method with which the processes in micro-contacts are successfully simulated[5].

19.2 Reduction of Contact Problems from Three Dimensions to One Dimension

Now, we will discuss a simulation method that is especially well suited for simulation of friction between rough surfaces. The laws of friction obtained using this method can subsequently be used in macroscopic system dynamics simulations. We limit ourselves to "typical tribological systems" which are characterized by the laws of dry friction being approximately met, especially, that the frictional force is approximately proportional to the normal force. This implies that the real contact area remains much smaller than the apparent contact area.

For "typical tribological systems," there is a series of properties that allow immense simplification of the contact problem and in this way, allow quick calculation even in multi-scaled systems. The simplifying properties used in the reduction method are the following:

(a) For velocities much smaller than the speed of sound[6], deformations can be treated as quasi-static;

(b) The potential energy, and therefore, the force-displacement relation, is a local property that depends only on the configuration of the micro-contacts and not the form or size of the body;

(c) The kinetic energy, on the other hand, is a "global property" that depends only on the form and size of the body as a whole and not on the configuration of the micro-contacts;

(d) Many significant properties in contact mechanics can be well approximated using one-dimensional systems, which allows for crucial reduction in calculation time.

These four properties are found in many macroscopic tribological systems. The application area of the subsequent methods is, accordingly, very wide. One must not forget that when applying these methods, the above conditions must be met. In the following, we will discuss the aforementioned simplifying assumptions in detail.

---

[5] V.L. Popov, und S.G. Psakhie, Numerical simulation methods in tribology. Tribology International, 2007, v. 40(6), pp. 916-923.

[6] This condition is met rather well in most real tribological contacts.

19.3 Contact in a Macroscopic Tribological System

(a) Quasi-steady state

In most tribological systems, we are dealing with the movements of elements which have a relative velocity (30 m/s at the highest) that is much smaller than the speed of sound (a few thousand m/s). Under these conditions, one can consider the problem to be *quasi-static*. Even for unsteady processes, during which the entire system can no longer be considered to be in steady-state, the conditions for quasi-steady state are still met very well for individual micro-contacts. In calculating contact deformations, in an overwhelming majority of real applications, we can apply equilibrium conditions in order to calculate deformations and, therefore, use all of the results from static contact mechanics from the previous chapters.

(b) Elastic energy as a local property

As we saw in Chapter 7, under typical operating conditions for tribological systems, contact partners come into contact with each other in many small micro-areas, whose total surface area is much smaller than the apparent surface area. Under certain conditions, the individual contact points can be considered independent from one another.

We will investigate this property a little more in depth by calculating the potential energy of a deformed contact area. We consider a cylindrical indenter with the diameter D which is pressed a distance d into a body (Fig. 19.2).

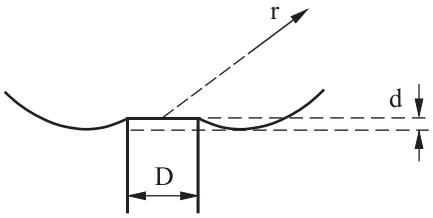

Fig. 19.2 Flat cylindrical indenter which is pressed a distance d into an elastic half-space.

The displacement in the elastic body at a point at large distance r from the point of indentation is

$$u \simeq \frac{D \cdot d}{r}. \tag{19.9}$$

The deformation can be estimated as $\varepsilon \simeq \frac{du}{dr} \simeq -\frac{D \cdot d}{r^2}$ and the energy density as $\mathrm{E} \simeq \frac{1}{2} G\varepsilon^2 \simeq \frac{1}{2} G \frac{D^2 \cdot d^2}{r^4}$. The elastic energy is found through integrating

$$U \simeq \int G \frac{D^2 \cdot d^2}{r^4} \pi r^2 dr = \pi G D^2 \cdot d^2 \int \frac{dr}{r^2}. \tag{19.10}$$

This integral converges at the upper limit. Since the asymptote (19.9) is only valid for $r > D$, the lower limit must be on the order of D (the integral would diverge for the lower limit of 0). The elastic energy is, therefore, concentrated in a volume with linear dimensions on the order of D – a result that we have already used in all of the estimations in the earlier chapters. In other words:

> The elastic energy is a local quantity that is only dependent on the configuration and deformation in the area near the micro-contact. The size and form of the macroscopic body is unimportant for the contact mechanics of this problem.

If the distance between the contact areas is much larger than their diameter, then they can be considered as being independent.

(c) Kinetic energy as a global property

The kinetic energy of a body behaves exactly the opposite. If a body impacts an indenter with the diameter D at a velocity v_0 much smaller than the speed of sound (Fig. 19.3), leading to a penetration at the velocity v_0, then the velocity field in a reference frame moving at v_0 has an order of magnitude of

$$v(r) = \frac{D \cdot \dot{d}}{r} = \frac{D v_0}{r} . \tag{19.11}$$

In the laboratory systems, the total kinetic energy of the body is calculated as

$$\begin{aligned} K &\approx \frac{1}{2}\int \rho \left(v_0 - \frac{v_0 D}{r} \right)^2 dV \approx \frac{1}{2}\int \rho v_0^2 dV - \int \rho v_0^2 \frac{D}{r} dV \\ &\approx \frac{1}{2} m v_0^2 - \int \rho v_0^2 \frac{D}{r} 2\pi r^2 dr \approx \frac{1}{2} m v_0^2 \left(1 - \frac{D}{R} \right). \end{aligned} \tag{19.12}$$

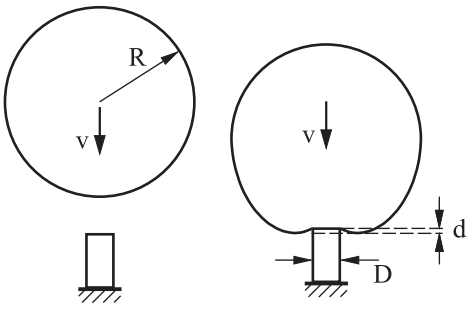

Fig. 19.3 A sketch for investigating the kinetic energy of a solid elastic body which impacts a rigid cylindrical indenter at a velocity v_0.

If the diameter of the contact area is much smaller than the size of the body, then the kinetic energy is equal to $mv_0^2/2$ by neglecting the first order terms of D/R.

The kinetic energy is a "non-local" property that is independent from the contact configuration, in a first order approximation, and can be assumed to be equal to the energy of the "rigid movement" of the body as a whole.

We have already implicitly used this property, for example, in the calculation of the time of impact between a sphere and a wall.

We come to the conclusion that the inertial properties of a macroscopic system under "typical conditions" are correctly described in treating the body as a rigid mass m. Its elastic properties, on the other hand, are completely determined by the stiffness of its micro-contacts. This approach is schematically presented in Fig. 19.4.

The inertial properties of three-dimensional systems are completely decoupled from contact properties under the majority of existing conditions. The former are completely *macroscopic*, while the latter are completely *microscopic*. *It is this decoupling that makes it possible for us to consider the frictional forces as surface forces in macroscopic system dynamics*.

This property, by the way, is not self-evident and would not be valid in a two-dimensional system for example. In the two-dimensional case, instead of having (19.10) we would have the integral $\int dr/r$, which diverges logarithmically at both limits. In the two-dimensional case, the elastic contact energy is, therefore, dependent on the contact configuration as well as the size and form of the body. The same is also valid for the kinetic energy.

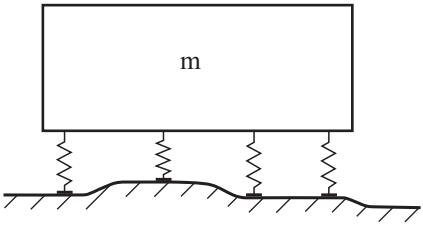

Fig. 19.4 The inertial properties of a macroscopic system under "typical conditions" can be correctly described using a rigid mass m. Its elastic properties, on the other hand, are completely determined by the (non-linear) stiffness of its contacts.

Now, we want to use the advantage that we live in a three-dimensional world and, according to this, assume the scale separation of the kinetic and potential energy for multi-contact problems.

(d) Dimension reduction of contact problems

Another crucial property of contacts between three-dimensional bodies is the close similarity between these contacts and certain one-dimensional problems. The fundamental ideas of this analogy are presented in the following. If a round indenter is pressed into the surface of an elastic continuum, then the stiffness of the contact is *proportional to its diameter* D (Equation 5.11):

$$c = DE^* . \tag{19.13}$$

This property can be reproduced using a one-dimensional *elastic foundation* (Fig. 19.5 a). In order to fulfill Equation (19.13), the stiffness per unit length must be chosen as E^*. Every individual spring must have the stiffness

$$\Delta c = E^* \Delta x . \tag{19.14}$$

If a "sphere" with the radius R_1 is brought into contact with the elastic foundation (penetration depth d), seen in Fig. 19.5, then the following contact quantities result: the contact radius is equal to

$$a = \sqrt{2R_1 d} \tag{19.15}$$

and the normal force is

$$F_N(d) = \frac{4\sqrt{2}E^*}{3}\sqrt{R_1 d^3} . \tag{19.16}$$

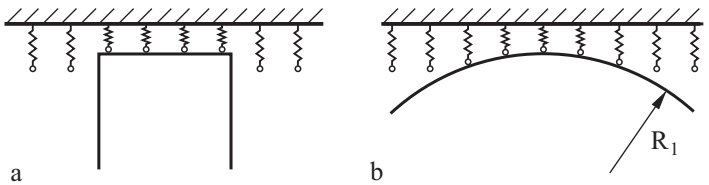

Fig. 19.5 One-dimensional elastic foundation in contact with a "cylindrical" indenter and a "sphere."

If we choose a radius

$$R_1 = R/2 , \tag{19.17}$$

then the Equations (19.15) and (19.16) coincide exactly with Hertzian theory.

The contact of a rotationally symmetric three-dimensional rigid body with an elastic continuum can be represented by the contact of a corresponding one-dimensional cross-section having half the radius of curvature with an elastic foundation having the stiffness per unit length of E^*.

This rule is *exactly* correct for *every* cylindrical indenter and for *every* parabolic body with an *arbitrary* radius of curvature.

Since a contact between an ellipsoid and a rigid plane can be approximated by a contact between a sphere and a plane (using the Gaussian radius $\sqrt{R^{(1)}R^{(2)}}$, see (5.30)), the representation of a non-rotationally symmetric contacts in a one-dimensional system is possible as well. Thereby, the Hertzian relation between normal force and contact area is still valid. The stiffness of indenters with non-circular cross-sections (5.13) shows that one-dimensional representation also works for bodies with square or triangular cross-sections with an error of less than 3%. The "one-dimensional diameter" of the contact, in this case, is calculated according to the rule $D = \left(4A/\pi\right)^{1/2}$.

The *tangential stiffness* of a three-dimensional contact is also proportional to the diameter of the contact:

$$c_{\perp} \approx \frac{4G}{2-\nu} \cdot 2a \,, \tag{19.18}$$

and thus, can be replicated using a one-dimensional elastic foundation for the same reasons. The tangential stiffness of individual springs in the elastic foundation must be chosen according to

$$\Delta c_{\perp} = \frac{4G}{2-\nu} \Delta x \,. \tag{19.19}$$

The fact that the force-penetration depth and the force-contact area relationships are independent of scaling for very different rotationally symmetric and non-symmetric individual contacts allows us to draw the hypothesis that this would also be the case with a randomly rough surface.

19.4 Reduction Method for a Multi-Contact Problem

In order to cross over to a contact between bodies with rough surfaces, a rule for the production of a one-dimensional profile, which is equivalent to the three-dimensional body in a contact mechanical sense, must be formulated (Fig. 19.6). As the motivation for this replacement, we use a few ideas from the model of Greenwood and Williamson. The results and quality of the replacement system, however, prove to be much better than the Greenwood-Williamson model itself.

In the model of Greenwood and Williamson, the individual contacts are considered to be independent from each other. Under these conditions, only the *distribution* of the *heights* of the asperities and the *radii of curvature* play a role. So, our goal is first to generate a one-dimensional system, which has the necessary statistical distributions of heights and radii of curvature.

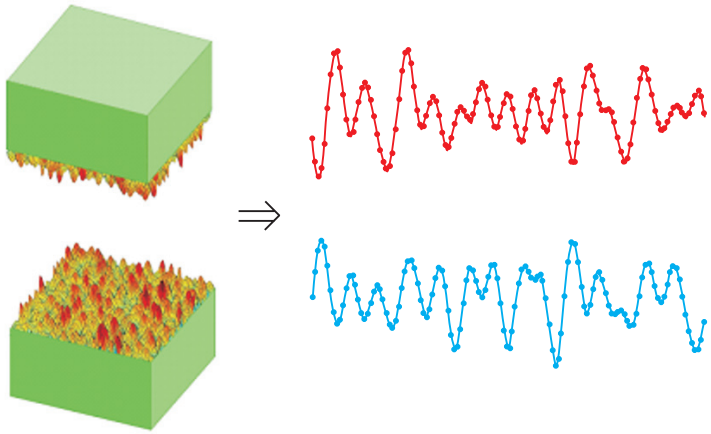

Fig. 19.6 Replacing two three-dimensional bodies with two equivalent one-dimensional "rough lines."

To simplify matters, we assume that the topography of the two-dimensional surface (of a three-dimensional body) can be unambiguously characterized by its *power spectrum* $C_{2D}(\vec{q})$, which is defined according to

$$C_{2D}(\vec{q}) = \frac{1}{(2\pi)^2} \int \left\langle h(\vec{x}) h(\vec{0}) \right\rangle e^{-i\vec{q}\cdot\vec{x}} d^2x \,, \tag{19.20}$$

where $h(\vec{x})$ is the height profile taken from the average so that $\langle h \rangle = 0$; $\langle . \rangle$ means averaging over the statistical ensemble. Furthermore, we assume that the surface topography is statistically homogeneous and isotropic. Under these conditions, the power spectrum $C_{2D}(\vec{q})$ is only dependent on the magnitude q of the wave vector $\vec{q}$.

Similarly, the power spectrum $C_{1D}(q)$ of a one-dimensional "surface" – a "rough line" is introduced:

$$C_{1D}(q) = \frac{1}{2\pi} \int \left\langle h(x) h(0) \right\rangle e^{-iqx} dx \,. \tag{19.21}$$

The surface topography is calculated in the two-dimensional case with the help of the power spectrum according to

$$h(\vec{x}) = \sum_{\vec{q}} B_{2D}(\vec{q}) \exp\left(i\left(\vec{q}\cdot\vec{x} + \phi(\vec{q})\right)\right), \tag{19.22}$$

with

$$B_{2D}(\vec{q}) = \frac{2\pi}{L}\sqrt{C_{2D}(\vec{q})} = \overline{B}_{2D}(-\vec{q}) \tag{19.23}$$

and the phases $\phi(\vec{q}) = -\phi(-\vec{q})$, which are randomly distributed on the interval $[0, 2\pi)$.

In the one-dimensional case, we have

$$h(x) = \sum_q B_{1D}(q)\exp\left(i\left(qx + \phi(q)\right)\right), \tag{19.24}$$

with

$$B_{1D}(q) = \sqrt{\frac{2\pi}{L}C_{1D}(q)} = \overline{B}_{1D}(-q). \tag{19.25}$$

Quick numerical methods are based on the *fast Fourier transform* (FFT) instead of direct calculation of the sums (19.22) or (19.24).

Theoretical considerations and numerical studies lead to the following transformation rules from a two-dimensional to a one-dimensional power spectrum:

In order to produce a one-dimensional system with the same contact properties as the three-dimensional system, the one-dimensional power spectrum must be used according to the rule

$$C_{1D}(q) = \pi q C_{2D}(q). \tag{19.26}$$

Qualitative arguments for this rule are the following: the average of the squares of the heights for the two-dimensional and one-dimensional cases, respectively, are

$$\left\langle h^2 \right\rangle_{2D} = 2\pi\int_0^\infty qC_{2D}(q)\,dq, \tag{19.27}$$

$$\left\langle h^2 \right\rangle_{1D} = 2\int_0^\infty C_{1D}(q)\,dq. \tag{19.28}$$

They are the same when $C_{1D}(q) = \pi q C_{2D}(q)$. The corresponding root mean squares of the curvature $\left\langle \kappa^2 \right\rangle$ also coincide in this case[7]. In the work[8] it was shown that the lines generated in this way are actually equivalent to the three-dimensional body regarding their contact mechanical properties. In particular, the height distribution of the one-dimensional "surfaces" with the power spectrum in

[7] For two-dimensional cases, we define $\kappa^2 = \kappa^{(1)}\kappa^{(2)}$, where $\kappa^{(1)}$ and $\kappa^{(2)}$ are the principal radii of curvature of the surface.

[8] T. Geike and V.L. Popov, Mapping of three-dimensional contact problems into one dimension. Phys. Rev. E., 2007, v. 76, 036710 (5 pp.).

(19.26) coincide with the height distribution of the two-dimensional surface, while the average radius of curvature of the peaks in the one-dimensional system is half as large as that of the three-dimensional system and this is exactly the ratio that is needed for the contact properties to perfectly coincide! Therefore, we have the correct force-displacement relationship as well as the force-contact area relationship.

As an example, a contact between two three-dimensional bodies with randomly generated rough surfaces was investigated. For the calculation, surfaces with 64×64 points were generated. The interrelation between the normal force and the real contact area was calculated with the boundary element method (Fig. 19.7). With the one-dimensional power spectrum calculated according to (19.26), the one-dimensional "rough line" was generated. This rough line was pressed into a rigid line and the lengths l_i of the *connected regions* were determined. From this, the contact area was *defined* according to the rule

$$A_{c,1D} = \frac{\pi}{4} \sum_j l_j^2 \ . \tag{19.29}$$

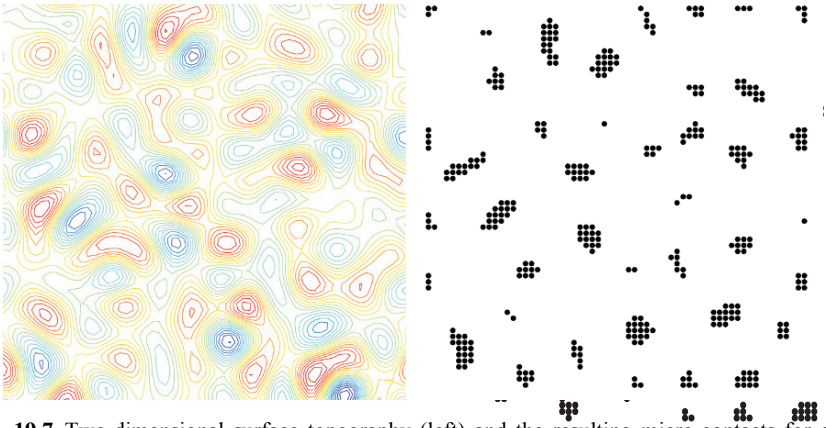

Fig. 19.7 Two-dimensional surface topography (left) and the resulting micro-contacts for one value of normal force (right) – results of a numerical calculation using the boundary element method.

All of the results were averaged over 450 random realizations of the surface. The dependence of the entire surface on the normal force is compared in Fig. 19.8 for a three-dimensional system and a one-dimensional system. The one and three-dimensional results excellently coincide for rough surfaces as well.

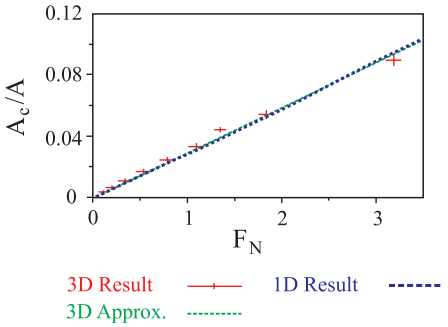

Fig. 19.8 Relation between relative contact area (A_c is real contact area, A apparent contact area) and normal force F. Three-dimensional results (Error bars based on 450 surfaces and thin dashed line for linear approximation of mean values) are compared to one-dimensional results (thick dotted line). One-dimensional result and linear approximation of three-dimensional results are difficult to distinguish because they match very closely.

From this, it follows that:

> Individual contacts for rotationally symmetric and non-rotationally symmetric three-dimensional rigid bodies as well as for random rough surfaces with an elastic continuum can be presented using a contact of an appropriate one-dimensional profile with an elastic foundation having a stiffness per unit length equal to E^*. This is valid in terms of force-displacement relationships, force-contact area relationships, as well as in terms of force-contact length relationships.

Let it be noted that the elastic foundation was earlier used by many researchers "as a last resort." The success of this model is based on the strong analogy described above between three-dimensional contacts and contacts with elastic foundations.

19.5 Dimension Reduction and Viscoelastic Properties

For viscoelastic bodies such as rubber, the contact can only be seen as quasi-static when the penetration velocity and the sliding velocity are smaller than the smallest speed of sound (which corresponds to the smallest modulus of elasticity). If this condition is met and an area of an elastomer is excited at a frequency ω, then there is a linear relation between the force and displacement with stiffness that is proportional to the contact radius. Hence, this system can also be presented using a one-dimensional system, where the stiffnesses of the individual springs must be chosen according to (19.14). Rubber can be considered as a incompressible medium, so that $\nu = 1/2$ and

$$\Delta c \approx E^*(\omega)\Delta x = \frac{E(\omega)}{1-\nu^2}\Delta x = \frac{2G(\omega)}{1-\nu}\Delta x = 4G(\omega)\Delta x\,. \tag{19.30}$$

In the case of rubber, the stiffness of the individual "springs" of the elastic foundation is four times the shear modulus multiplied with the mesh spacing.

In the one-dimensional model, the stress-strain relation (15.2) must be replaced by

$$\tilde{F}_i(t) = 4\Delta x \int_{-\infty}^{t} G(t-t')\dot{\delta}(t')dt'\,. \tag{19.31}$$

19.6 Representation of Stress in the Reduction Model

As long as the bodies are only elastically or viscoelastically deformed, one needs no information about the resulting stresses in the contact area. However, if the bodies are plastically deformed or worn due to stress peaks, then information about the stress occurring in the contact is necessary for the simulation. In the one-dimension model, only the *spring forces* are directly defined, not the stresses. In the following, it will be shown that in the 1D model, a stress can also be defined that coincides with Hertzian stress distribution in the case of elastic deformation.

The force in a spring is

$$\tilde{F}_i = \Delta x E^* \delta_i = \Delta x E^* \left(d - \frac{x_i^2}{2R_1} \right), \tag{19.32}$$

where δ_i is the displacement of the spring i and Δx is the mesh spacing. Now, we *define* the stress as

$$\sigma_i = \frac{\tilde{F}_i}{b\sqrt{\delta_i R_1}}\,. \tag{19.33}$$

Here, b is the constant still to be determined. The stress is dependent on the radius of curvature and is, therefore, a non-local quantity[9].

[9] The following arguments can be cited as motivation for this form of the stress: the contact radius for an individual contact is equal to $a = \sqrt{2\delta R}$, where δ is the penetration depth. We have an approximation for the average stress of $\sigma \propto \frac{F_N}{a^2} \propto \frac{F_N / a}{a} \propto \frac{\langle \tilde{F}_i \rangle}{\sqrt{R\delta}}$, where $\langle \tilde{F}_i \rangle$ is the average spring force in the contact area. This is exactly the form (19.33). The fact that using the coordi-

From (19.33), (19.32), and (19.16) we get:

$$\sigma_i = \frac{3\sqrt{2}}{4}\frac{F_N}{a^2}\frac{\Delta x}{b}\sqrt{1-\frac{x_i^2}{a^2}}\,. \tag{19.34}$$

For a Hertzian spherical contact, the stress distribution is equal to

$$\sigma = \frac{3F_N}{2\pi a^2}\sqrt{1-\frac{x^2}{a^2}}\,. \tag{19.35}$$

These two stress distributions coincide when

$$b = \frac{\pi\sqrt{2}}{2}\Delta x\,. \tag{19.36}$$

Thus, the stress is calculated from the local spring force $\tilde{F}_i$ and the local deformation δ_i according to

$$\sigma_i = \frac{\tilde{F}_i\sqrt{2}}{\pi\Delta x\sqrt{\delta_i R_1}}\quad . \tag{19.37}$$

For the yield criterion, the non-local quantity σ_i according to Equation (19.37) should be used, rather than the local force $\tilde{F}_i$.

19.7 The Calculation Procedure in the Framework of the Reduction Method

The calculation procedure for the reduction method consists of the following steps:

1. The frictional surface is measured (e.g. using a white light interference microscope or an atomic force microscope).
2. The two-dimensional power spectrum of the surface is calculated with the fast Fourier transform.
3. This is now transformed into the one-dimensional power spectrum according to the rule in (19.26).
4. With this power spectrum, a one-dimensional “rough line” is generated which has the same contact properties as the original three-dimensional system.
5. The elastic properties are chosen according to the rule in (19.14).

---

nate-dependent penetration depth δ_i leads exactly to the Hertzian stress distribution can be considered an empirical discovery.

6. The bodies are pressed onto one another and moved relative to one another in the tangential direction. The ratio of the average tangential force to the average normal force is the coefficient of friction.
7. In addition to the coefficient of friction, the total real contact area, the total contact length (simply the sum $L = \sum_j l_j$), as well as their distributions, the average stress, and the stress distribution in the contact can be calculated.

19.8 Adhesion, Lubrication, Cavitation, and Plastic Deformations in the Framework of the Reduction Method

The reduction method can be expanded in order to take adhesion, lubrication, and cavitation in lubricated contacts into account. Particulars to this method can be found in the literature recommended for this chapter (see the section entitled "Further Reading").

Problems

Problem 1: Formulate an algorithm for calculating the coefficient of friction between a rigid surface with a given surface topography and a smooth viscoelastic body that can be modeled using the rheological model consisting of a spring connected in parallel to a velocity proportional damper.

Solution:
1. The profile of the rigid surface $h(x, y)$ is the input data and must first be measured (Fig. 19.9) and saved in the form of a two-dimensional array.

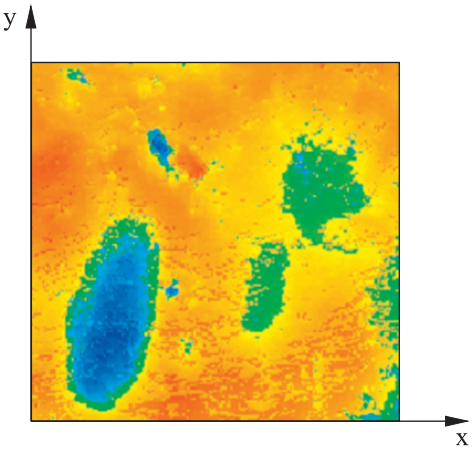

Fig. 19.9 Example of a surface topography measurement.

2. With the help of the FFT, the Fourier transform $B(q_x, q_y)$ of the surface profile is calculated (Fig. 19.10) and afterwards, the power spectrum: $C_{2D}(q_x, q_y) = \left(\frac{L}{2\pi}\right)^2 \left|B_{2D}(q_x, q_y)\right|^2$.

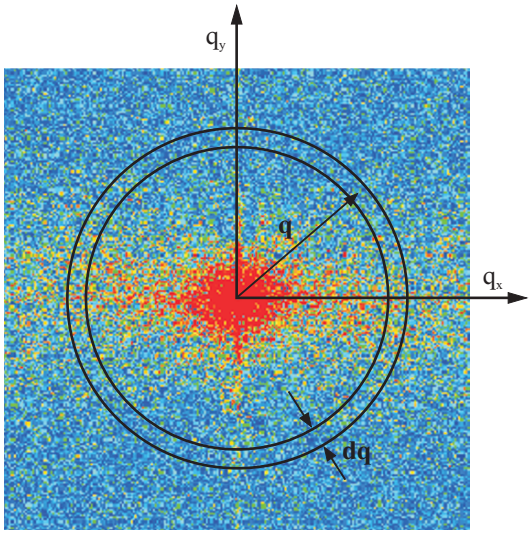

Fig. 19.10 Power spectrum of the profile shown in Fig. 19.9.

3. Now, the spectrum is averaged over a circle with the radius q and the same discretization interval dq (Fig. 19.10). The result is the angular-independent power spectrum $C_{2D}(q)$.

4. An equivalent one-dimensional power spectrum is calculated according to (19.26): $C_{1D}(q) = \pi q C_{2D}(q)$.

5. With this power spectrum, a one-dimensional profile is generated using Equation (19.24) and taking Equation (19.25) into account. This profile represents the initial two-dimensional surface in the following calculations.

6. To verify the correctness, the root mean square Δh_{2D} of the original two-dimensional surface and Δh_{1D} of the generated one-dimensional surface are calculated. Their averaged values over several realizations must coincide.

7. Now, we get to the dynamic simulation. We define the zero level of the rigid rough line as zero on the z-axis (Fig. 19.11). The rigid line is discretized at the beginning with the mesh spacing Δx with which it was produced. Its profile in the discretization points is given by h_i. The level of the undisturbed surface of the viscoelastic material we denote as Z_0. The line representing the viscoelastic material is discretized using the same mesh spacing Δx with which the rigid rough line was generated.

8. The roughness profile moves to the left with the velocity v: $h(x,t) = h(x+vt)$. The values in the discrete points are: $h_i(t_n) = h(i\Delta x + vn\Delta t)$, where n is the number of time steps.

9. The interaction relation between the rough surface and the viscoelastic material is defined: (a) the rigid surface is impenetrable for the viscoelastic material; (b) if a point of the viscoelastic material were displaced by Δz_i and its velocity equals $\Delta \dot{z}_i$, then a force according to (19.30) would act on the point:

$$f_i = 4G\Delta x \Delta z_i + 4\eta \Delta x \Delta \dot{z}_i,$$

where G is the shear modulus of the (three-dimensional) viscoelastic material and η is its viscosity; (c) this force cannot be negative (no adhesion).

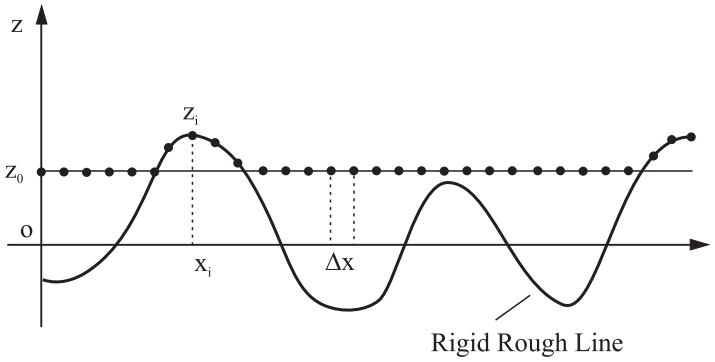

Fig. 19.11 One-dimensional substitute model for the contact between a viscoelastic material and a rough rigid surface.

10. The system is "initialized" by placing the viscoelastic material "near" the rigid line: that means at a distance of about $3\Delta h_{1D}$ from the zero line. Thereby, those points of the body meeting the condition $h_i \geq Z_0$ come into contact with the rough substrate. We initially set the force acting on the system to be equal to $f_i = 4G\left(h_i - Z_0\right)$. The total force acting on the viscoelastic material is equal to

$$F = \sum_{\substack{\text{points}\\ \text{in}\\ \text{contact}}} f_i = 4G\Delta x \sum_{\substack{\text{points}\\ \text{in}\\ \text{contact}}} \left(h_i - Z_0\right).$$

In the vertical direction, a normal force $-F_N$ is applied.

11. Choice of time step: In the time Δt, the upper body is always displaced by a discretized step of Δx. Thus, the time step is

$$\Delta t = \Delta x / v .$$

12. Time loop: In the next state (displaced by Δx), the condition $h_i(t_{n+1}) \geq z_i$ is checked and in this way, the *new points that have come into contact* are determined. The force acting on these points is calculated using

$$f_i(t_{n+1}) = 4G\Delta x\left(h_i(t_{n+1}) - Z_0\right) + 4\eta\Delta x\left(h_i(t_{n+1}) - z_i(t_n)\right)/\Delta t .$$

For the points that were in contact in the previous step, it is initially assumed that they remain on the surface: therefore, their coordinates change from $z_i(t_n) = h_i(t_n)$ to $z_i(t_{n+1}) = h_i(t_{n+1})$. The force is calculated using the same formula. If the force is positive, then the points remain in contact. If it is negative, then these points are said to have lost contact and force acting on them is set to zero.

For all points that are not in contact, their new position is determined using the condition that

$$G\cdot\left(z_i\left(t_n\right) - Z_0\right) + \eta\frac{z_i\left(t_{n+1}\right) - z_i\left(t_n\right)}{\Delta t} = 0 .$$

From this, it follows that

$$z_i\left(t_{n+1}\right) = z_i\left(t_n\right) - \frac{G}{\eta}\cdot\Delta t\left(z_i\left(t_n\right) - Z_0\right).$$

Thereby, the total force acting on the material would be equal to

$$F = \sum_i f_i(t_{n+1}) = \sum_i 4G\Delta x\left(h_i(t_{n+1}) - Z_0\right) + 4\eta\Delta x\left(h_i(t_{n+1}) - z_i(t_n)\right)/\Delta t ,$$

which is summed over all of the points found to be in contact.

Since, the normal force should remain constant, the state of the upper surface Z_0 changes so that the total vertical force is F_N. To achieve this, the body is displaced by ΔZ. The force resulting from this movement is equal to

$$\Delta F = -\Delta Z \sum_i \left(4G\Delta x + 4\eta\Delta x / \Delta t\right) = -\Delta ZN\left(4G\Delta x + 4\eta\Delta x / \Delta t\right).$$

Here, N is the number of points in contact. Together with the force calculated in the previous step, it must result in exactly F_N:

$$-\Delta ZN\left(4G\Delta x + 4\eta\Delta x / \Delta t\right) + F = F_N.$$

From this, it follows that

$$\Delta Z = \frac{F - F_N}{N\left(4G\Delta x + 4\eta\Delta x / \Delta t\right)}, \quad Z_0(t_{n+1}) = Z_0(t_n) + \Delta Z.$$

13. In order to calculate the tangential force, the normal force acting on the point i is multiplied with the tangent of the inclination angle of the surface:

$$f_{x,i} = f_i \frac{h_{i+1} - h_{i-1}}{2\Delta x}$$

and summed over *all* contacts:

$$F_x = \sum_{\substack{\text{points} \\ \text{in} \\ \text{contact}}} f_i \frac{h_{i+1} - h_{i-1}}{2\Delta x}.$$

14. The ratio F_x / F_N is the instantaneous value of the coefficient of friction. Averaged over the total time, it provides us the average coefficient of friction.